A Novel Hybrid Energy Storage System Using the Multi-Source Inverter

Lea Dorn-Gomba, *Student Member, IEEE,* Ephrem Chemali, *Student Member, IEEE,* and Ali Emadi, *Fellow, IEEE*
Electrical and Computer Engineering Department
McMaster University, Hamilton, ON, Canada
Email: dorngoml@mcmaster.ca

***Abstract*—This paper introduces a new active Hybrid Energy Storage System (HESS) topology which utilizes the multi-source inverter to interconnect a battery and an ultracapacitor directly to the three-phase load without the use of any additional power electronic converters or DC/DC converters. A new control strategy has been developed which periodically switches the operating mode of the multi-source inverter at a high frequency in order to maintain smooth current sharing. A duty cycle can also be selected to bias the use of one energy storage device over another which enables control over the discharge rate of the two sources. Closed-loop control simulations for an Urban Dynamometer Driving Schedule (UDDS) with torque and speed references driving an electric machine have been performed to verify the operation principle of this novel HESS topology. The influence of the additional control parameters on the source currents and their State of Charge (SOC) has been further investigated through simulations. Moreover, experiments in open-loop control with a scaled-down prototype and a R-L load have been carried out and validated the theoretical influence of the new control on the input DC currents. By an appropriate choice of the new control parameters, the average battery current and the battery current ripple can be reduced by up to 90% and 60% respectively compared to traditional electrified powertrains that only uses a single energy source.**

***Index Terms*—Battery control, electric vehicles, hybrid energy storage systems, Li-ion batteries, multi-source inverters, ultracapacitors.**

I. Introduction

Contemporary electric drive vehicles utilize Li-ion batteries to meet the load demands of the electric motor. Li-ion batteries have a high energy density allowing for longer electric only driving range but they do not offer high power densities. Although their power rating might meet the peak load requirements of a vehicle, higher C-rates exhibited by the battery are found to reduce battery lifetime [1]. As a result, requiring the battery to meet highly dynamic load profiles increases the rate of unwanted side reactions which, in turn, results in further plating of the solid-electrolyte interface [2]–[4]. This translates into an increase in the internal resistance which reduces its lifespan or can even lead to premature failure. In contrast to Li-ion batteries, ultracapacitors (UC) offer larger power densities but at the cost of lower energy densities.

A Hybrid Energy Storage System (HESS) harnesses the benefits of both Li-ion batteries and UC by pairing these two energy sources together [5]–[8]. These devices have been the subject of much research since they alleviate the peak load demand which is otherwise requested from the battery bank. Therefore, the battery is left to provide most of the constant load demand while the power dense UC bank supplies the peak power profile. In turn, the battery wear is minimized which allows the battery's lifetime to be maximized [9]–[11]. In addition, since the cost of the battery is one of the most expensive component of an electric drive vehicle, an additional benefit of HESS is the ability to reduce the size and therefore the cost of the battery pack.

In a conventional active HESS topology, such as the parallel HESS circuit shown in Fig. 1-a, a DC/DC converter aims to control the source currents in order to use the battery for most of the constant power while the UC meets dynamic load profiles [12]–[15]. Moreover, it enables the control of the charge and discharge rates of the two sources. As a result, the battery lifetime can be extended and the efficiency of the system is improved. However, even if active HESS topologies achieve promising performance and offer more controllability compared to passive HESS structures, they are still held back from commercial applications. Indeed, their use in traction drive systems is mainly limited by the high cost, extra weight and large volume of the DC/DC converter.

The fundamental concept of the multi-source inverter has been introduced in [16]–[18]. This power converter aims to generate distinct output line-to-line voltages from several DC sources using a single stage conversion. Unlike multilevel inverters that can provide numerous output voltages as a ratio of the shared DC input voltage, the multi-source inverter directly uses the independent input sources to provide the output voltage levels [19]. Thus, different DC sources such as generators, batteries or DC renewable energy sources can be connected to the same AC output. This topology has been first developed for hybrid and plug-in hybrid electric powertrains where a battery pack and an engine provide power to the wheels [20]–[24]. With the multi-source inverter, the battery can directly drive a motor without stepping up its voltage with a DC/DC boost converter. Thus, when applied to hybrid and plug-in hybrid electric powertrains, the power rating of this DC/DC converter can be decreased and the overall efficiency of the electrified powertrain can be improved since no additional conversion stage is used between the battery and the motor.

978-1-5386-1180-7/18/$31.00 ©2018 IEEE

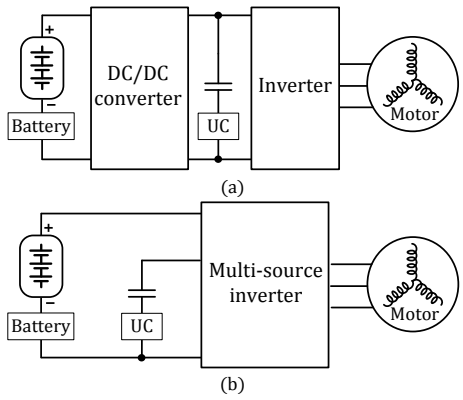

Fig. 1: (a) Parallel active HESS topology. (b) Proposed active HESS topology with the multi-source inverter.

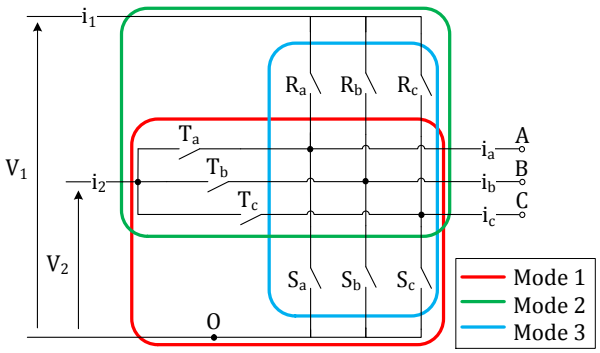

Fig. 2: Multi-source inverter topology with two sources.

This paper presents a new activate HESS topology which couples Li-ion batteries to UC through the multi-source inverter (Fig. 1-b). Because of the specific current distribution of this inverter, an innovative control scheme has been developed to regain current sharing between the sources, as it is traditionally done with active HESS topologies. Hence, an active control of the input sources and their current is achieved without the use of a DC/DC converter. Therefore, the combination of a battery-UC HESS topology with the multi-source inverter intends to keep the advantages of an active HESS without the drawbacks of a DC/DC converter.

The following will first introduce the multi-source inverter with its operating modes. Then, the active HESS topology with the multi-source inverter is presented and the novel control scheme managing the current distribution between the two sources is detailed. Simulations in closed-loop control with an interior permanent magnet (IPM) synchronous machine for an Urban Dynamometer Driving Schedule (UDDS) have been performed to verify the theoretical principles of operation of the proposed topology. Finally, the impact of the new control strategy on the sources is further investigated and shown through simulations and experiments.

II. Multi-source inverter

The multi-source inverter is a topology that aims to connect several DC-link sources to a three-phase load. It has been previously studied as a new option for electrical propulsion system architectures in hybrid and plug-in hybrid vehicles. In this case, two DC sources, namely V_1 and V_2, are connected and it can be seen from Fig. 2 that the multi-source inverter consists of three different two-level inverters. By replacing the ideal switches $R_{a,b,c}$, $S_{a,b,c}$ and $T_{a,b,c}$ by IGBTs, the multi-source inverter circuit is very similar to the Neutral Point Clamped (NPC) or T-NPC topologies [17], [18]. The main difference lies in the connection between the upper and lower switches in each leg of the inverter. Indeed, in a typical three-level inverter, the upper and lower sides are connected to a neutral point which generates an additional DC-bus voltage level equal to zero. Thus, the voltage across the input series-connected capacitors is one-half of the DC input voltage. On the contrary, there is no neutral point in the multi-source inverter. The input sources are decoupled and each input capacitor voltage is identical to the source voltage across it.

According to the state of the switches of Fig. 2, three distinct voltages can be applied to the output line-to-line voltages, implying three operating modes:

- Mode 1: the switches $S_{a,b,c}$ and $T_{a,b,c}$ enable V_2 to supply the motor and V_1 is not used;
- Mode 2: the switches $R_{a,b,c}$ and $T_{a,b,c}$ enable V_1 to supply the motor while charging V_2. The voltage applied to the output is equal to $V_1 - V_2$;
- Mode 3: the switches $R_{a,b,c}$ and $S_{a,b,c}$ enable V_1 to supply the motor and V_2 is not used.

The voltages [V_{AO}, V_{BO},V_{CO}] can be defined as functions of the state of the switches and the input voltages:

$$\begin{aligned} V_{AO} &= C_{Ra}V_1 + C_{Ta}V_2 - Z_a.i_a \\ V_{BO} &= C_{Rb}V_1 + C_{Tb}V_2 - Z_b.i_b \\ V_{CO} &= C_{Rc}V_1 + C_{Tc}V_2 - Z_c.i_c \end{aligned} \quad (1)$$

where Z_i is the phase impedance of the load, $i = a, b$ or c is the corresponding phase and $C_{Ra,b,c}$ and $C_{Ta,b,c}$ are the switching functions of the switches $R_{a,b,c}$ and $T_{a,b,c}$ respectively.

In a similar manner, the input currents [i_1,i_2] can be expressed as follows:

$$\begin{aligned} i_1 &= C_{Ra}.i_a + C_{Rb}.i_b + C_{Rc}.i_c \\ i_2 &= C_{Ta}.i_a + C_{Tb}.i_b + C_{Tc}.i_c \end{aligned} \quad (2)$$

As a result, the different combinations of the switches enable up to seven distinct line-to-line voltages if two DC sources are connected to the multi-source inverter (Table I).

An adapted Space Vector Pulse Width Modulation (SVPWM) has been developed based on the similarities of the multi-source inverter with three-level inverters. The theoretical operation of the adapted SVPWM has been already presented in [17], [18] and will not be repeated in this paper.

TABLE I: Switching combinations of the multi-source inverter.

Modes	States of switches									Line-to-line voltages		
	R_a	R_b	R_c	S_a	S_b	S_c	T_a	T_b	T_c	V_{AB}	V_{BC}	V_{CA}
1	Always open			0	1	1	1	0	0	V_2	0	$-V_2$
				0	0	1	1	1	0	0	V_2	$-V_2$
				1	0	1	0	1	0	$-V_2$	V_2	0
				1	0	0	0	1	1	$-V_2$	0	V_2
				1	1	0	0	0	1	0	$-V_2$	V_2
				0	1	0	1	0	1	V_2	$-V_2$	0
2	1	0	0	Always open			0	1	1	$V_1 - V_2$	0	$-(V_1 - V_2)$
	1	1	0				1	0	0	0	$V_1 - V_2$	$-(V_1 - V_2)$
	0	1	0				1	0	1	$-(V_1 - V_2)$	$V_1 - V_2$	0
	0	1	1				1	0	0	$-(V_1 - V_2)$	0	$V_1 - V_2$
	0	0	1				1	1	0	0	$-(V_1 - V_2)$	$V_1 - V_2$
	1	0	1				0	1	0	$V_1 - V_2$	$-(V_1 - V_2)$	0
3	1	0	0	0	1	1	Always open			V_1	0	$-V_1$
	1	1	0	0	0	1				0	V_1	$-V_1$
	0	1	0	1	0	1				$-V_1$	V_1	0
	0	1	1	1	0	0				$-V_1$	0	V_1
	0	0	1	1	1	0				0	$-V_1$	V_1
	1	0	1	0	1	0				V_1	$-V_1$	0

III. Active HESS topology using the multi-source inverter

The multi-source inverter has been implemented in an active HESS topology where a battery and an UC supply power to the motor (Fig. 1-b). Like all other active HESS structures, the proposed topology needs to efficiently control the source currents in order to take advantage of the high energy density of batteries as well as the large specific power and cycle life of UCs, while minimizing battery degradation.

As previously mentioned, the multi-source inverter has three distinct operating modes that can be employed. When a closed-loop speed-torque control strategy is applied, the proportional integral (PI) controllers generate a voltage reference that is used in the adapted SVPWM to determine the operating mode and decide which source drives the wheels. Hence, the two sources never supply power to the motor simultaneously and the DC current provided to the load is equal to either the battery current or the UC current. This prevents the use of a similar control strategy than in a conventional parallel HESS where the DC input current of the inverter is equal to the sum of the currents from the two sources. Thus, applying a speed-torque control to the motor without any additional control of the sources is not sufficient to obtain similar performance as with an active HESS architecture.

A novel control scheme has been developed in order to manage the current distribution in the proposed active HESS topology with the multi-source inverter. Simulations in closed-loop control over an UDDS will be presented in the following to verify its principle of operation.

A. Control of the system

An active control of the multi-source inverter′s operating modes can be combined with the speed-torque control scheme in order to effectively manage the current distribution between the two sources. This additional mode control has two degrees of freedom, namely, the control frequency f_c and the discharge duty cycle d_c, representing the conduction time during which the battery supplies power to the load. The fundamental purpose of the mode control is to periodically switch the operating mode between Modes 1 and 3, regardless of the mode determined by the speed-torque control strategy. Thus, the load demand will be regularly met by either the battery current or the UC current. Furthermore, with an appropriate choice of f_c, the input capacitor banks will filter the source currents to prevent them from being discontinuous. Thereby, over one control period ($1/f_c$), the average input current supplying the motor will be the sum of the source currents just like with a typical parallel HESS. Moreover, since the discharge duty cycle biases the use of one energy source over another, it can control the average source currents and, hence, the discharge rate of the sources. Over one control period, the average battery current $\langle i_{bat} \rangle$ and the average UC current $\langle i_{uc} \rangle$ can be expressed as functions of the average input current $\langle i_{in} \rangle$ that supplies the load and the discharge duty cycle d_c,

$$\begin{aligned} \langle i_{bat} \rangle &= d_c . \langle i_{in} \rangle \\ \langle i_{uc} \rangle &= (1 - d_c) . \langle i_{in} \rangle \end{aligned} \tag{3}$$

The control scheme of the active HESS topology using the multi-source inverter is shown in Fig. 3. The speed, torque and mode controls act simultaneously and aim to impact on the adapted SVPWM without impeding the performance of the overall system.

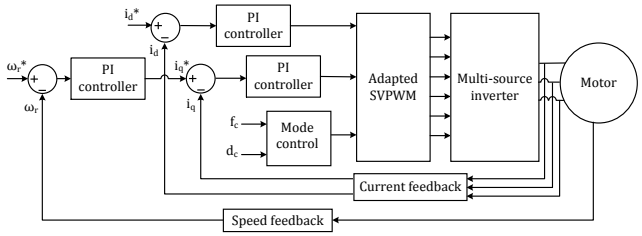

Fig. 3: Control scheme of the active HESS topology using the multi-source inverter.

As a result, this new control scheme regains current sharing

TABLE II: Simulation parameters of the DC sources.

Source	Cells in series & parallel	Maximum power density (kW/kg)	Energy density (Wh/kg)
Battery	81 & 6	3.13	173.9
UC	105 & 1	13.7	7.7

between both sources and discharge rate regulation, as it is traditionally done with active HESS topologies. Moreover, it intends to achieve similar performance, with the additional benefit of not using a DC/DC converter.

B. Simulations of the system

The proposed active HESS topology with the multi-source inverter has been modeled in Matlab/Simulink. The Li-ion battery model used in this work is a first-order equivalent circuit model. The model has been parameterized using experimental cell test data for an SOC-OCV curve and a pulse discharge test for a Batterist lithium polymer battery cell (PF9744128). Ultracapacitors have a lower internal resistance than Li-ion batteries and hence have a shorter time constant. The UC model used in this work includes leakage current and equivalent series resistance [25]. The SOC-OCV relationship is presumed to be linear as a result of the lack of faradaic reactions occurring in UC [25], [26]. The capacitance and the two resistance values are based on the Maxwell BCAP3400 ultracapacitor [27]. The SOC of the UC is found by utilizing the linear SOC-OCV relationship [28], [29].

Closed-loop control simulations were performed for an UDDS with torque and speed references driving an IPM. A 10 Hz control frequency f_c and a discharge duty cycle d_c of 50% have been selected in the mode control. The switching frequency of the multi-source inverter is 10 kHz and has been independently chosen from the control frequency f_c. As mentioned earlier, the first order equivalent circuit model and parameterization were performed at the cell level. The number of cells in series and parallel in the battery and UC packs are scaled according to the power requested at the DC bus (Table II). In turn, parameter fitting and characterization of the full pack model render the cell stack parameters.

Simulation results are shown in Figs. 4 and 5. From Figs. 4 (a) and (b), it can be seen that the rotor speed and torque converge to the references. This verifies that the additional mode control strategy does not hinder the performance of the system. Figs. 4 (c) and (d) show the voltages of the two sources and their SOC. Even if a discharge duty cycle of 50% does not bias one source to another, the UC voltage and SOC drops are larger compared to the battery pack. This can be explained by the fact that the UC energy density is much lower than for the battery. Thus, it will discharge faster for a similar load current. Hence, an effective choice of the discharge duty cycle needs to consider the energy density of the sources in order to avoid their full discharge in a short period of time. Fig. 5 shows the current distribution according to the operating mode. In Fig. 5-b, the reference current corresponds to the input current when the mode control is not applied and only one source drives the

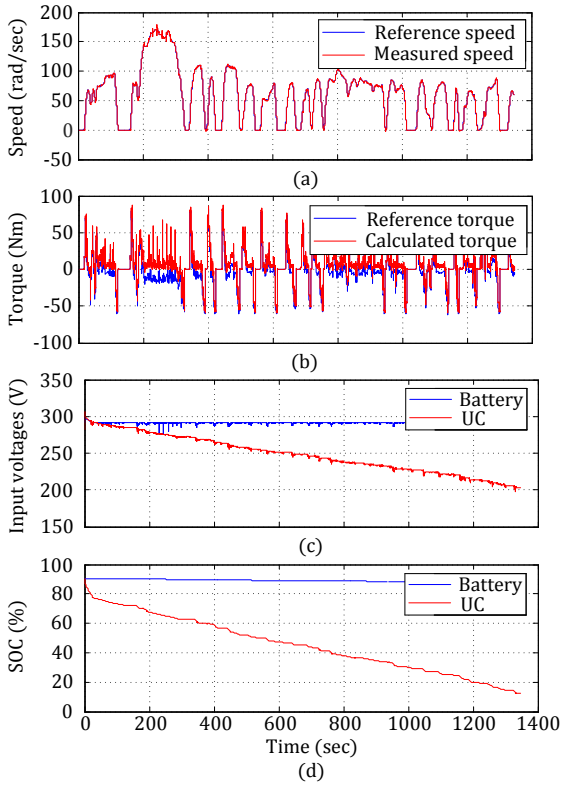

Fig. 4: Simulation results: (a) Rotor speed. (b) Torque. (c) Input DC voltages. (d) SOC of the sources.

motor. The battery and UC currents have been obtained when the mode control is used with a discharge duty cycle of 50% and f_c equal to 10 Hz. When either one of the sources supplies power to the motor, its input current is equal to the reference current while it remains null when the source is not used. This leads to discontinuous currents with high ripples, which is not suitable for the battery lifetime. This discontinuity is due to the choice of a low control frequency f_c that prevents the currents from being filtered by the input capacitors. Further details will be provided in section IV.

IV. Influence of the Mode Control Parameters

From the previous part, it has been shown that the additional mode control does not impede the performance of the speed and torque controls. However, a low control frequency f_c leads to discontinuous currents, which is not suitable for the lifetime of the battery. Moreover, choosing a discharge duty cycle of 50% pointed out the lower energy density of the UC. This will affect the choice of the discharge duty cycle since it can impact on the discharge rate of the sources. The influence of the control frequency f_c and the discharge duty cycle d_c on the input currents and the SOC of the sources are discussed in the following section.

A. Influence of the control frequency f_c

Input capacitor banks are used to protect the DC-link voltage from transient spikes and minimize ripple currents caused

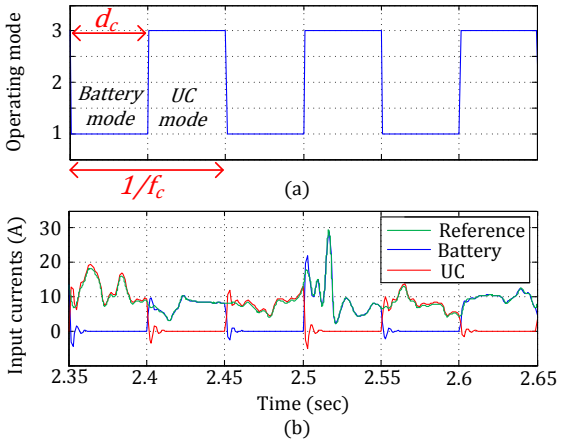

Fig. 5: (a) Operating modes. (b) Reference, battery and UC currents.

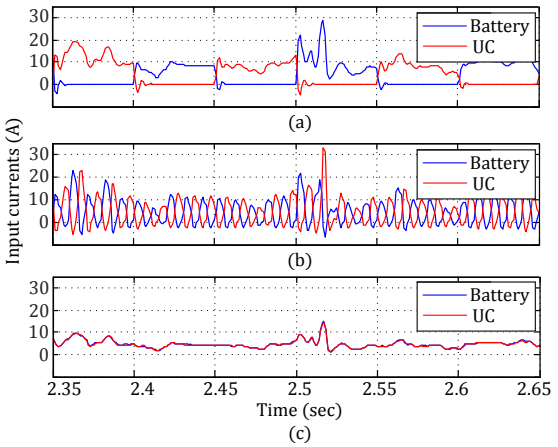

Fig. 6: Influence of f_c on the battery and UC currents for: (a) 10 Hz. (b) 100 Hz. (c) 5 kHz.

by the switching circuits. They act as low-pass filters and allow the low frequency signals while blocking those with high frequencies. The new control scheme for the proposed active HESS topology with the multi-source inverter aims to take advantage of these input filters to smooth the source currents. Indeed, by an appropriate choice of f_c, high frequency source currents can be generated in order to be filtered by the input capacitors. As a result, the source currents will be continuous and their ripple will be reduced.

Closed-loop control simulations for three different values of f_c with a constant discharge duty cycle of 50% were performed for a shorted time UDDS with torque and speed references driving an IPM. In the simulation model, input capacitor banks of 3 mF have been selected and a parasitic resistance of 0.1 Ω is considered. Thus, the cut-off frequency of these input filters is equal to 530 Hz. The battery and the UC current waveforms are shown in Fig. 6. As expected, it can be seen that increasing f_c smooths the currents. Since the cut-off frequency is equal to 530 Hz, input currents for f_c equal to 10 Hz are not filtered and thus discontinuous (Fig. 6-a). Fig. 6-b shows currents with a medium frequency of 100 Hz. The signals start being filtered which is characterized by continuous waveforms with large oscillations. Finally, Fig. 6-c presents the current waveforms for f_c equal to 5 kHz. The high frequency signals are completely filtered by the input capacitors which can be seen by the low current ripple.

From these simulation results, it can be concluded that choosing a high f_c smooths the input currents, which is particularly beneficial for the battery in order to extend its lifetime.

B. *Influence of the discharge duty cycle* d_c

Since the discharge duty cycle biases one source to another, it is intuitively expected that it will impact on the average currents and the SOC of the sources.

Closed-loop control simulations for several discharge duty cycles with a constant control frequency f_c of 5 kHz were performed for a shorted time UDDS with torque and speed references driving an IPM. From Fig 7, it can be seen that the average current and ripple of the battery become smaller when the discharge duty cycle decreases. On the other hand, a low discharge duty cycle increases the UC average current and its ripple. This is due to the fact that decreasing the discharge duty cycle reduces the conduction time of the battery while the UC is used for a longer time during one mode control period. Fig. 8 shows the SOC of the battery and the UC for a control frequency f_c of 5 kHz at different discharge duty cycles. Increasing the discharge duty cycle leads to larger SOC drop for the battery and lower SOC drop for the UC. Since the SOC is calculated as a function of the current, these results are consistent with those from Fig. 7.

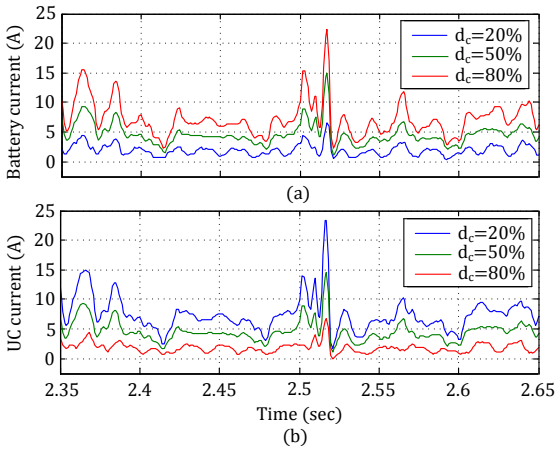

Fig. 7: Influence of d_c on the current (a) Of the battery. (b) Of the UC.

C. *Experimental results*

A scaled-down prototype was built to validate the influence of the new control parameters f_c and d_c on the input DC currents (Fig. 9). The control of the gate signals of the multi-

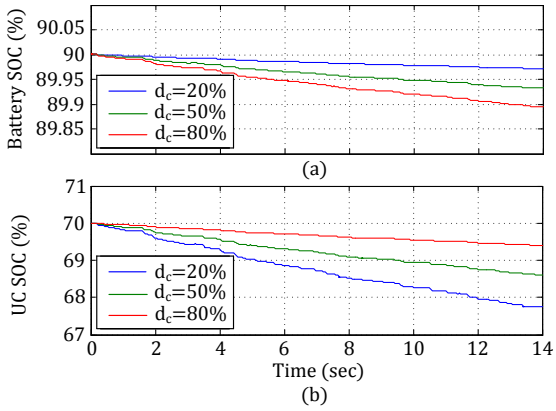

Fig. 8: Influence of d_c on the SOC (a) Of the battery. (b) Of the UC.

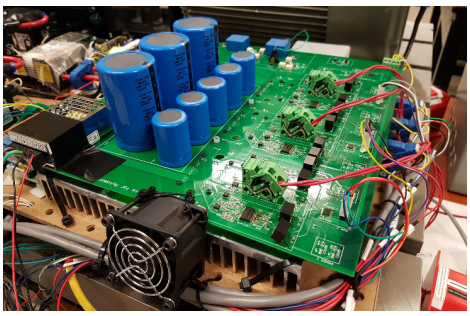

Fig. 9: Prototype of the multi-source inverter.

source inverter are managed by a MicroAutoBox II and the software dSPACE. Open-loop control experiments with a R-L load were performed and the battery and UC voltages were provided by two power supplies. The parameters are presented in Table III. In the following results, the same operating point has been tested for different f_c and d_c.

In Fig. 10, the input currents i_{bat} and i_{uc} and the phase current i_a are shown for a discharged duty cycle fixed at 50% and a control frequency f_c of 10 Hz, 100 Hz and 5 kHz. It can be seen that, as the frequency increases, both input currents become continuous and their ripple is also reduced. Indeed, in Figs. 10 (a) and (b), i_{bat} and i_{uc} are discontinuous and their ripple is high, while smooth current sharing is achieved for a high frequency f_c of 5 kHz thanks to the input capacitor banks that act as low-pass filters (Fig. 10-c). From Fig. 11, the currents i_{bat}, i_{uc} and i_a are displayed for a constant control frequency f_c of 5 kHz and a discharge duty cycle of 20% and 80%. By choosing a discharge duty cycle lower than 50%, the

TABLE III: Experiment parameters.

Parameters	Value
Battery and UC voltages	150 V
Switching frequency	10 kHz
R-L load	5Ω and $256\mu H$

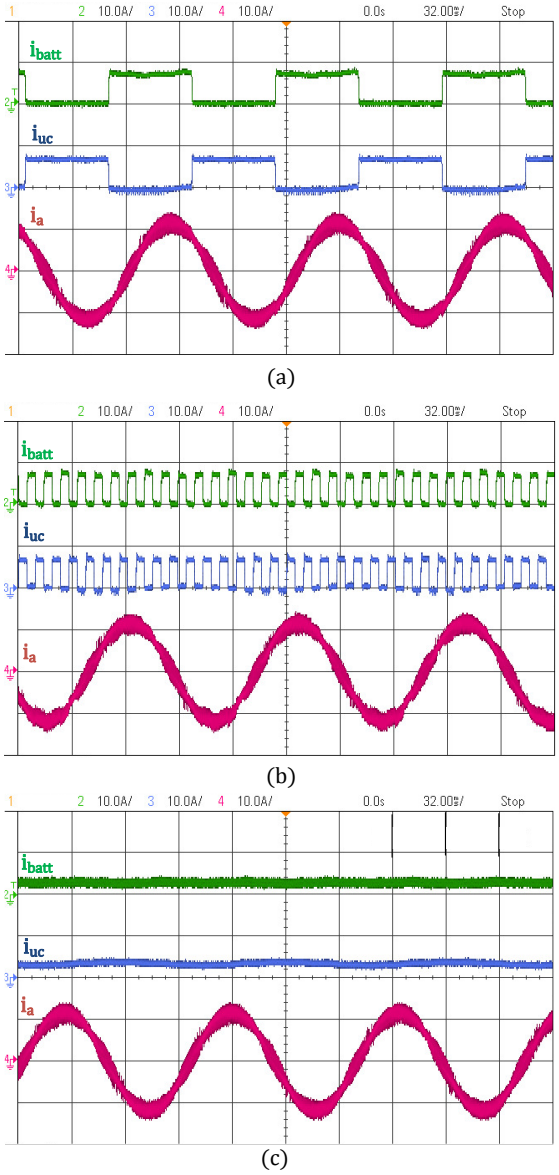

Fig. 10: Current waveforms of i_{bat}, i_{uc} and the phase i_a for $d_c = 50\%$ and (a) $f_c = 10Hz$. (b) $f_c = 100Hz$. (c) $f_c = 5kHz$.

UC provides more power than the battery which can be seen from a higher average current (Fig. 11-a). On the contrary, the average battery current will be greater than the average UC current if d_c is greater than 50% (Fig. 11-b). On the other hand, in both Figs. 10 and 11, the phase current i_a is sinusoidal with a constant amplitude and frequency regardless of the variation of f_c or d_c. This validates the fact that the additional mode control does not interfere with the control of the load.

As a result, the experimental results are consistent with the theoretical operation principle of the new control strategy of the multi-source inverter and validate the influence of both parameters f_c and d_c.

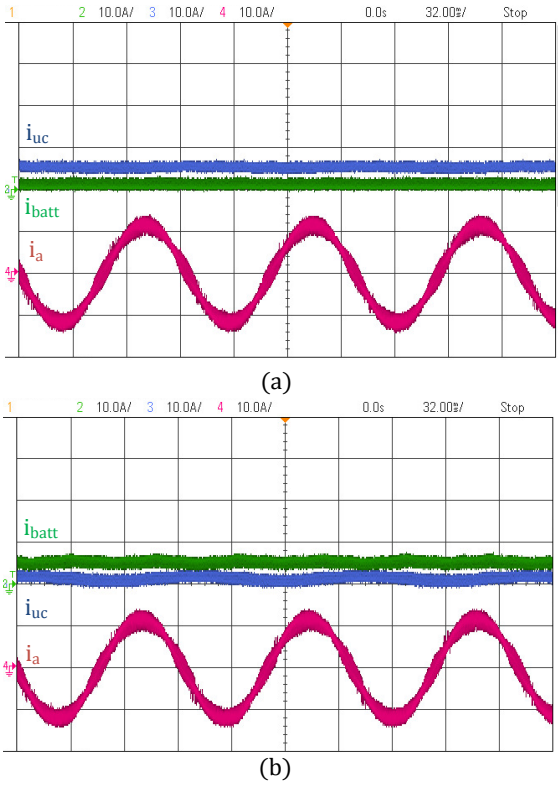

Fig. 11: Current waveforms of i_{bat}, i_{uc} and the phase i_a for $f_c = 5kHz$ and (a) $d_c = 20\%$. (b) $d_c = 80\%$.

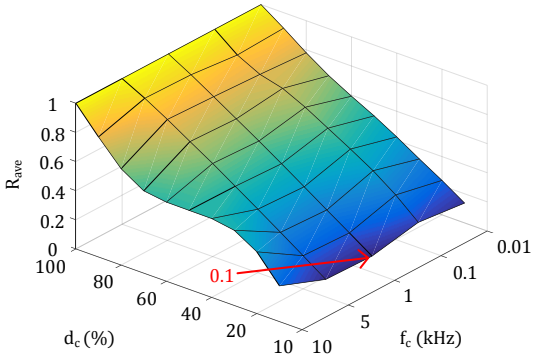

Fig. 12: Ratio R_{ave} depending on f_c and d_c.

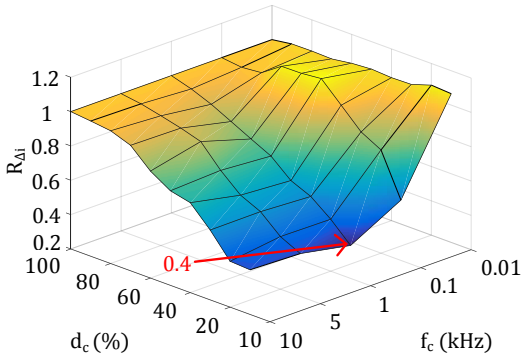

Fig. 13: Ratio $R_{\Delta I}$ depending on f_c and d_c.

D. Influence of the mode control parameters on the battery

One solution to extend the battery lifetime is to control its average current and reduce its current ripple. The following graphs summarize the effects of the control mode parameters on these two battery current variables.

The absolute value of the battery current has been averaged in order to consider positive and negative currents since they both adversely affect the battery lifetime. A ratio of the time-average value R_{ave} is calculated as below,

$$R_{ave} = \frac{\langle i_{bat} \rangle}{\langle i_{ref} \rangle} \quad (4)$$

where $\langle i_{bat} \rangle$ is the average battery current and $\langle i_{ref} \rangle$ is the average reference current. The reference current has been previously introduced in Fig. 5 and corresponds to the case where the mode control is not applied and only one source drives the motor. Hence, the ratio R_{ave} points out the average battery current reduction that can be achieved compared to the reference case for a specific control frequency f_c and discharge duty cycle d_c.

In Fig. 12, it can be seen that a low discharge duty cycle leads to a low ratio R_{ave}. In other terms, decreasing the discharge duty cycle reduces the average battery current, which is consistent since the battery is less used. Moreover, it can be seen that the control frequency f_c has a moderate impact on R_{ave}.

The current ripple can be calculated as the difference between the maximum and the minimum current values. A ratio of the battery current ripple $R_{\Delta I}$ is given by,

$$R_{\Delta I} = \frac{\Delta i_{bat}}{\Delta i_{ref}} \quad (5)$$

where Δi_{bat} and Δi_{ref} are the battery and reference current ripples, respectively.

The ratio $R_{\Delta I}$ is also a function of f_c and d_c and indicates the battery current ripple reduction which can be achieved relative to the reference case. It can be seen in Fig. 13 that increasing the control frequency f_c significantly reduces the battery current ripple. A low discharge duty cycle also leads to larger reduction of the battery current ripple which is due to the sharing with the UC.

Finally, one can note that R_{ave} and $R_{\Delta I}$ reach the values 0.1 and 0.4 respectively for a discharge duty cycle d_c of 10%. In other terms, the average battery current and the battery current ripple can be reduced by up to 90% and 60% respectively, compared to traditional electrified powertrains that only uses a single energy source. However, it should be kept in mind that, even if a low discharge duty cycle and high control frequency seem more suitable to preserve the battery lifetime, it also leads to a faster discharge of the UC. Therefore, a trade-off needs to be made to minimize the ripple and average battery current while ensuring sufficient SOC rates for both sources. The optimization of the new control parameters will

be investigated in the future.

V. Conclusion

This paper presents a new active HESS topology which couples a battery to an UC through the multi-source inverter. An innovative control scheme has been developed to actively control the operating mode of the inverter and aims to achieve similar performance than a typical HESS architecture with the additional benefit of not using a DC/DC converter. Indeed, thanks to the input capacitors that act as low-pass filters, smooth current sharing is achieved by periodically switching the operating mode at high frequency. Moreover, a duty cycle can also be selected to bias the use of one energy storage device over another which enables control over the discharge rate of the two sources. Closed-loop control simulations have been performed to verify that the additional mode control strategy does not hinder the performance of the system. Moreover, the influence of the mode control parameters has been analyzed and validated through open-loop control experiments with a scaled-down prototype and a R-L load. Finally, the influence of the new control on the battery has been studied and showed that the average battery current and the battery current ripple could be reduced by up to 90% and 60% respectively, compared to traditional electrified powertrains that only uses a single energy source.

Acknowledgement

This research was undertaken, in part, thanks to funding from the Canada Excellence Research Chairs (CERC) Program.

References

[1] R. Ahmed, M. E. Sayed, I. Arasaratnam, J. Tjong, and S. Habibi, "Reduced-Order Electrochemical Model Parameters Identification and SOC Estimation for Healthy and Aged Li-Ion Batteries. Part II: Aged Battery Model and State of Charge Estimation," *IEEE Journal of Emerging and Selected Topics in Power Electronics*, vol. 2, no. 3, pp. 678–690, 2014.

[2] ——, "Reduced-Order Electrochemical Model Parameters Identification and SOC Estimation for Healthy and Aged Li-Ion Batteries. Part I: Aged Battery Model and State of Charge Estimation," *IEEE Journal of Emerging and Selected Topics in Power Electronics*, vol. 2, no. 3, pp. 659–677, 2014.

[3] I. J. Fernández, C. F. Calvillo, A. Sánchez-Miralles, and J. Boal, "Capacity fade and aging models for electric batteries and optimal charging strategy for electric vehicles," *Energy Journal*, vol. 60, pp. 35–43, 2013.

[4] L. Lam and P. Bauer, "Practical capacity fading model for Li-ion battery cells in electric vehicles," *IEEE Trans. on Power Electron.*, vol. 28, no. 12, pp. 5910–5918, 2013.

[5] S. Pay and Y. Baghzouz, "Effectiveness of battery-supercapacitor combination in electric vehicles," in *IEEE Bologna PowerTech*, vol. 3, Bologna, Italy, Jun 2003, pp. 728–733.

[6] A. Kuperman, I. Aharon, S. Malki, and A. Kara, "Design of a semiactive battery-ultracapacitor hybrid energy source," *IEEE Trans. on Power Electron.*, vol. 28, no. 2, pp. 806–815, 2013.

[7] B. Hredzak, V. Agelidis, and M. Jang, "A Model Predictive Control System for a Hybrid," *IEEE Trans. On Power Electron.*, vol. 29, no. 3, pp. 1469–1479, 2014.

[8] A. Emadi, *Advanced Electric Drive Vehicles*, 1st ed. CRC Press, 2015.

[9] S. M. Lukic, S. G. Wirasingha, F. Rodriguez, J. Cao, and A. Emadi, "Power management of an ultracapacitor/battery hybrid energy storage system in an hev," in *Vehicle Power and Propulsion Conference, (VPPC'06)*, Windsor, UK, Sept 2006, pp. 1–6.

[10] J. Cao and A. Emadi, "A New Battery/UltraCapacitor Hybrid Energy Storage System for Electric, Hybrid, and Plug-In Hybrid Electric Vehicles," *IEEE Trans.on Power Electron.*, vol. 27, no. 1, pp. 122–132, 2012.

[11] A. Ostadi, M. Kazerani, and S. K. Chen, "Hybrid Energy Storage System (HESS) in vehicular applications: A review on interfacing battery and ultra-capacitor units," in *IEEE Transportation Electrification Conference and Expo*, Detroit, MI, USA, Jun 2013.

[12] A. Kuperman, I. Aharon, S. Malki, and A. Kara, "Design of a semiactive battery-ultracapacitor hybrid energy source," *IEEE Trans. on Power Electron.*, vol. 28, no. 2, pp. 806–815, 2013.

[13] J. Cao and A. Emadi, "A new battery/ultracapacitor hybrid energy storage system for electric, hybrid, and plug-in hybrid electric vehicles," *IEEE Trans.on power electron.*, vol. 27, no. 1, pp. 122–132, 2012.

[14] E. Chemali, L. McCurlie, B. Howey, T. Stiene, M. M. Rahman, M. Preindl, R. Ahmed, and A. Emadi, "Minimizing battery wear in a hybrid energy storage system using a linear quadratic regulator," in *Industrial Electronics Society, IECON 2015-41st Annual Conference of the IEEE*, Yokohama, Japan, Nov 2015, pp. 003 265–003 270.

[15] E. Chemali, M. Preindl, P. Malysz, and A. Emadi, "Electrochemical and electrostatic energy storage and management systems for electric drive vehicles: State-of-the-art review and future trends," *IEEE Journal of Emerging and Selected Topics in Power Electronics*, vol. 4, no. 3, pp. 1117–1134, 2016.

[16] A. Emadi and P. Magne, "Power Converter," Patent U.S. 0 117 770 A1, May 1, 2014.

[17] L. Dorn-Gomba, P. Magne, C. Barthelmebs, and A. Emadi, "On the concept of the multi-source inverter," in *Applied Power Electronics Conference and Exposition (APEC)*, Long Beach, CA, USA, Mar 2016, pp. 453–459.

[18] L. Dorn-Gomba, P. Magne, B. Danen, and A. Emadi, "On the concept of the multi-source inverter for hybrid electric vehicle powertrains," *IEEE Trans. On Power Electron.*, pp. 1–1, 2017.

[19] H. Abu-Rub, J. Holtz, J. Rodriguez, and G. Baoming, "Medium-voltage multilevel converters state of the art, challenges, and requirements in industrial applications," *IEEE Trans. on Ind. Electron.*, vol. 57, no. 8, pp. 2581–2596, 2010.

[20] A. Emadi, S. S. Williamson, and A. Khaligh, "Power electronics intensive solutions for advanced electric, hybrid electric, and fuel cell vehicular power systems," *IEEE Trans. on Power Electron.*, vol. 21, no. 3, pp. 567–577, 2006.

[21] H. Ye, Y. Yang, and A. Emadi, "Traction Inverters in Hybrid Electric Vehicles," in *2012 IEEE Transportation Electrification Conference and Expo (ITEC)*, Dearborn, MI, USA, Jun. 2012, pp. 1–6.

[22] O. Hegazy, J. Van Mierlo, and P. Lataire, "Design and Control of Bidirectional DC/AC and DC/DC Converters for Plug-in Hybrid Electric Vehicles," in *2011 International Conference on Power Engineering, Energy and Electrical Drives (POWERENG)*, Malaga, Spain, May 2011, pp. 1–7.

[23] T. A. Burress, S. L. Campbell, C. L. Coomer, C. W. Ayers, A. A. Wereszczak, J. P. Cunningham, L. D. Marlino, L. E. Seiber, and H. T. Lin, "Evaluation of the 2010 Toyota Prius Hybrid Synergy Drive System," Oak Ridge National Laboratory, Tech. Rep., May 2011.

[24] H. Bai and C. Mi, "The Impact of Bidirectional DC-DC Converter on the Inverter Operation and Battery Current in Hybrid Electric Vehicles," in *2011 IEEE 8th International Conference on Power Electronics and ECCE Asia (ICPE ECCE)*, Jeju Province, South Korea, May 2011, pp. 1013–1015.

[25] Y. Fuyuan, L. Languang, Y. Yuping, and Y. He, "Characterization , Analysis and Modeling of an Ultracapacitor," *World Eletric Vehicle Journal*, vol. 4, pp. 358–369, 2010.

[26] C. FÇŐrcaÅ§, D. PetreuÅ§, I. Ciocan, and N. PalaghiÅčÇŐ, "Modeling and simulation of supercapacitors," *International Symposium for Design and Technology of Electronics Packages*, pp. 195–200, Sept 2009.

[27] Maxwell, "Datasheet - k2 ultracapacitors - 2.85v/3400f," Tech. Rep., 2014.

[28] S. E. Samadani, R. Fraser, and M. Fowler, "A Review Study of Methods for Lithium-ion Battery Health Monitoring and Remaining Life Estimation in Hybrid Electric Vehicles," *SAE International*, 2012.

[29] S. S. Lee, H. J. Kim, G. J. Han, D. Cho, and G. Deok, "A Study on the dynamic SOC compensation of an Ultracapacitor module for the Hybrid Energy Storage System," in *Telecommunications Energy Conference*, Incheon, Korea (South), Oct 2009, pp. 1–7.